Synchronous Electromagnetic Encoders Based on Step-Impedance Resonators

Amirhossein Karami-Horestani, *Member, IEEE,* Ferran Paredes, *Senior Member, IEEE,* and Ferran Martín, *Fellow, IEEE*

***Abstract*—This paper presents a new type of electromagnetic encoders based on step-impedance resonators (SIRs). The encoders consist of a linear chain of transversely oriented SIRs etched on a dielectric substrate, whereas the reader is a simple microstrip transmission line fed by a certain number of single-tone signals, i.e., three in one prototype, and four in another prototype, tuned to specific predefined frequencies. System functionality is based on detecting at which of such predefined frequencies (considering all possible combinations) each SIR of the chain resonates. Thus, the number of combinations (or states) per encoder position (or row) corresponding to the prototype fed with three single-tone signals is 7, whereas it is 15 for the prototype fed with four single-tone signals, corresponding to 2.81 bits and 3.91 bits, respectively, per encoder row. Although there are other synchronous electromagnetic encoders exhibiting a higher number of bits per row, the number of chains of those encoders is at least two, and the readers are complex microwave structures based on power splitters, contrary to the prototypes reported in this paper. Enhancing the number of bits per row in these encoders is a fundamental aspect towards the implementation of true absolute electromagnetic encoders able to determine the position relative to the reader at any instant of time without the need to know the previous stages of encoder motion (a need in the incremental-type and in the so-called quasi-absolute encoders).**

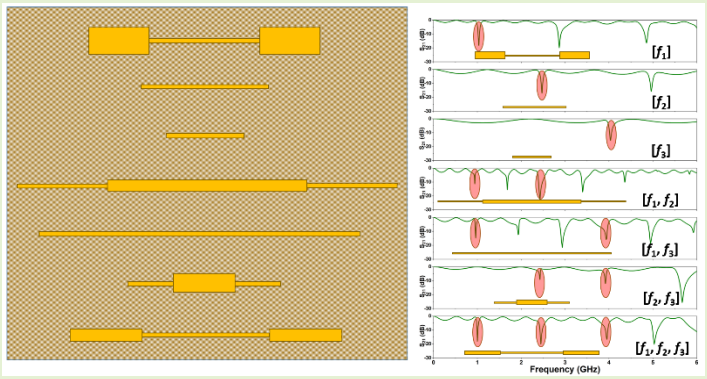

***Index Terms*— Electromagnetic encoder, displacement sensor, microstrip technology, microwave sensor, step-impedance resonator (SIR).**

I. Introduction

ELECTROMAGNETIC encoders have been recently proposed as an alternative to optical encoders [1]-[3] for motion sensing. The working principle of both types of encoders is similar, namely, the detection of certain elements conveniently arranged in the encoder, forming arrays or chains. In optical encoders, such elements are apertures, detected by means of optical beams. By contrast, electromagnetic encoders consist of a chain, or various chains, of metallic inclusions printed or etched in a dielectric substrate, and such inclusions (typically electrically small resonators or patches) are detected through electromagnetic radiation (microwaves) by near field [4],[5]. Nevertheless, in certain reported prototypes, the encoders are implemented as chains of dielectric inclusions embedded in a dielectric substrate [6]. As the inclusions, either apertures (in optical encoders) or metallic/dielectric elements (in the electromagnetic counterparts) cross the sensitive part of the reader (or stator), electrical pulses are generated, and the velocity and encoder position relative to the reader can be determined. There are many other approaches for the measurement of displacements and velocities by means of electromagnetic fields, including magnetic encoders [7],[8] and Hall-effect sensors [9]-[15], but such devices use magnets or coils, and are therefore costly, as compared to electromagnetic encoders.

Other low-cost microwave displacement sensors are based on the effects that metallic elements (typically planar resonators) generate in the response of a transmission line, or in a more complex microwave circuit, when such elements are in relative motion to such line or circuit [16]-[32]. Nevertheless, in this later type of displacement sensors, the input dynamic range is typically small, i.e., of the order of the dimensions of the element in motion. By contrast, in linear electromagnetic

This work was supported by MCIN/AEI 10.13039/501100011033, Spain, through the projects PID2019-103904RB-I00 (ERDF European Union) and PDC2021-121085-I00 (European Union Next Generation EU/PRTR), by the AGAUR Research Agency, Catalonia Government, through the project 2021SGR-00192, and by Institució Catalana de Recerca i Estudis Avançats (who awarded Ferran Martín). A. Karami-Horestani acknowledges MCIN/AEI /10.13039/501100011033 and ESF for Grant PRE2020-093239.

A. Karami-Horestani, F. Paredes, and F. Martín are with GEMMA/CIMITEC, Departament d'Enginyeria Electrònica, Universitat Autònoma de Barcelona, 08193 Bellaterra, Spain. (e-mail: Amirhossein.Karami@uab.cat).

encoders, the input dynamic range is unlimited, provided the encoder is equipped with a linear chain of inclusions that extends along the entire length of the encoder.

Electromagnetic encoders can be classified according to various criteria. For example, there are linear [6],[33-39] and rotary encoders [40]-[42], of application to the measurement of linear and angular displacements, respectively, and velocities.

Another categorization scheme distinguishes between incremental encoders [6],[33],[34],[40]-[42], quasi-absolute encoders [35]-[40], and absolute encoders [43]-[49]. In incremental electromagnetic encoders, the displacement is determined from the cumulative number of pulses from a reference (REF) position. Such encoders are implemented by means of a single periodic chain of inclusions, either linear or circular [6],[33],[34],[40]-[42]. The main limitation of such encoders is that after a system reset, it is necessary to return to the REF position in order to determine the relative displacement with regard to the reader. The solution to this limitation is provided by the absolute encoder systems, able to determine the position of the encoder regardless of its previous motion stages. In such electromagnetic encoder systems, each encoder position, or row, is identified with a unique identification (ID) code, and the number of bits for each row must be enough to discern all the different encoder positions, given by the ratio between the length of the encoder, L, and the period, p (which dictates the encoder resolution). Thus, the number of bits, n, should satisfy:

$$n \geq \log_2\left(\frac{L}{p}\right) \tag{1}$$

The main difficulty with absolute electromagnetic encoders comes from the fact that a significant number of bits might be necessary in high resolution (p small) long encoders (L high). Indeed, increasing the number of bits, n, in absolute encoders is a research challenge, and schemes based on frequency encoding [43]-[48] and phase encoding [49] have been recently proposed. For example, in [45], a single chain of metallic strips of different sizes (particularly, four) is considered, corresponding to 2 bits per encoder position, and the specific strip size is determined by feeding the reader (a transmission line with a series gap) with as many single tone signals as strip sizes. When one of the strips of the encoder is on top of the reader line, the corresponding single-tone signal is transmitted, as far as it is tuned to the resonance frequency of that strip, and the size (and hence the ID code for that position) can be determined. Other schemes based on frequency encoding (and inclusions' size) use various chains and complex readers based on power splitters [46],[47]. In [47], 8.78 bits per encoder position were achieved, a competitive number of bits, but at the expense of a reader implemented by means of a 4-output power splitter.

In a recent work, phase encoding for the implementation of absolute encoders was considered [49]. Specifically, such phase-modulation electromagnetic encoders consist of a linear chain of identical inclusions but located at different transverse positions with regard to the axis of the chain. When the encoder is displaced over the reader, a one-port transmission line terminated with a matched load and fed by a single-tone signal tuned to the resonance frequency of the inclusions (resonant strips in [49]), the phase of the reflection coefficient is dictated by the transverse position of the corresponding inclusion, and encoding is achieved. Four bits per encoder position were achieved in [49], by considering a single chain encoder. The sensitive element of the reader in such phase-modulation encoders is simple (a one-port transmission line terminated with a matched load), but retrieving the phase in a real scenario, by means of phase detectors, is not absent of certain difficulty [49].

Quasi-absolute encoders based on a binary encoding scheme were reported before the frequency and phase encoder systems highlighted in the two preceding paragraphs [35]-[40]. In such systems, one bit per encoder position is assigned, and encoder position is determined by reading the bit corresponding to the considered position, plus the $n - 1$ bits of the previous positions. By this means, a total of n bits satisfying (1) is enough to discern all the encoder positions, and for that purpose, it is necessary that the ID sub-code of any subset of adjacent n positions does not repeat (this is possible through encoding by means of the so-called De Bruijn sequence [50], as discussed in detail in [35]). The main problem with these quasi-absolute encoders, based on a binary scheme for encoder position, is that, after a system reset, the encoder must displace n periods to be able to provide the absolute encoder position. Thus, investigating schemes focused on enhancing the number of bits per encoder period compatible with simple readers, pursuing the implementation of absolute encoders, is of the highest interest in the field of electromagnetic encoders.

In this paper, we propose a radically new approach to implement synchronous electromagnetic encoders with more than one bit of information per encoder period. In one of the reported prototypes, 3.91 bits with a single encoder chain are achieved, and a simple reader, i.e., a transmission line fed by various single tone signals, is used. The paper is organized as follows. The new working principle of such encoders is presented in Section II. Section III is devoted to present the specific encoder inclusions considered, i.e., step-impedance resonators (SIRs), and the necessary theory to understand the strategy to conveniently tune the SIRs to the necessary resonance frequencies. Experimental validation is the subject of Section IV. Comparison with other electromagnetic encoders is discussed in Section V. Finally, the main conclusions are highlighted in Section VI.

II. Working Principle

In [45], encoders with 4 different inclusion (strip) sizes, and hence providing 2 bits of information per encoder period (or row), were considered. The specific inclusion size (state) of the row was detected by feeding the reader (a microstrip line with a series gap) with four single-tone signals tuned to the resonance frequencies of the four encoder strips. Only one amongst the four possible frequencies is activated per row. For that reason, the number of bits in such encoders is limited to $n = 2$. In the encoders proposed in this paper, the working principle consists in considering all the possible combinations of frequencies of the feeding signals per row, i.e., not simply

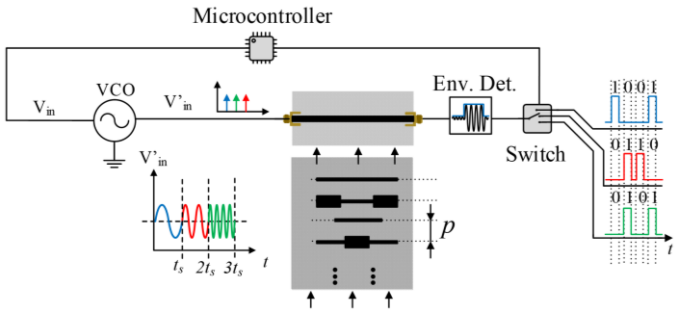

Fig. 1. Sketch showing the working principle of the proposed electromagnetic encoders.

activating one. Let us assume that the number of feeding signals is N. The number of possible combinations of frequencies, or states, excluding the case where none of the frequencies is activated is simply $2^N - 1$. Thus, the number of bits per encoder period, or row, is

$$n = \log_2(2^N - 1) \tag{2}$$

and $n \approx N$, provided N is high, or moderately high. By contrast in the encoder system reported in [45], the number of bits is

$$n = \log_2(N) \tag{3}$$

Thus, with the system proposed in this paper, a significant enhancement in the number of bits per row is possible.

The sketch of the proposed electromagnetic encoder system (optimized) is depicted in Fig. 1. The reader is a transmission line fed by N single-tone signals, managed by a microcontroller (which sequentially injects the signals in a time-division multiplexing scheme). The encoder must be implemented by means of a chain with inclusions able to resonate at any of the $2^N - 1$ frequency combinations of the feeding signals. For instance, for $N = 3$, the 7 different states must be implemented with 7 inclusions able to resonate at $[f_1]$, $[f_2]$, $[f_3]$, $[f_1, f_2]$, $[f_1, f_3]$, $[f_2, f_3]$, or $[f_1, f_2, f_3]$. The functionality of the encoder system is as follows. The encoder chain must be displaced over the reader line at short distance. When an inclusion is on top of the line, the feeding signal, or signals, tuned to the resonance frequency, or frequencies, of that inclusion, will be reflected back, generating a notch in the transmission coefficient. Thus, the specific state, among the $2^N - 1$ states, corresponding to that inclusion can be retrieved by means of an amplitude detector, similar to the approach presented in [45].

III. SIR-BASED ENCODERS

Selectively generating the resonance frequencies corresponding to all possible combinations is not simple. One possibility would be to consider a set of frequencies for the feeding signals, $f_1, f_2, \ldots, f_N$, satisfying that $f_i \neq m \cdot f_j$ (m being an integer, and $f_i > f_j$, with $i, j = 1, 2, \ldots, N$), i.e., non-harmonic signals. If multiples between the two frequencies of any pair are avoided, the encoder inclusions can be implemented, e.g., by means of as many planar resonant elements as frequencies. For example, for $N = 3$, the 7 states corresponding to the above-cited frequency combinations, i.e., $[f_1]$, $[f_2]$, $[f_3]$, $[f_1, f_2]$, $[f_1, f_3]$, $[f_2, f_3]$, or $[f_1, f_2, f_3]$, can be generated by selectively etching, or printing, in the encoder rows resonant elements with fundamental resonance frequencies tuned to f_1, f_2, and/or f_3, and choosing those that are required to generate the specific frequency combination. Planar microwave resonators typically exhibit harmonic frequencies (multiples of the fundamental one). Nevertheless, with the cited strategy, all frequency combinations are possible since the harmonic frequencies of the different resonators (three resonators for $N = 3$) do not coincide with the fundamental frequencies of the others. However, this approach has a fundamental limitation: the number of required resonators per encoder period in the worst case (note that N resonators are necessary for the combination $[f_1, f_2, \ldots, f_N]$). This approach is feasible, but at the expense of an increase of encoder size, as far as up to N resonators per row might be required, depending on the specific ID code of the row.

In this paper, a strategy different to the one based on multiple resonators with non-harmonic resonance frequencies is contemplated. A single resonator per encoder period, specifically a step-impedance resonator (SIR), is considered. The key aspect is that the topology of such resonator can be tailored in order to modify (engineer) the resonance frequencies, with the possibility of generating non-harmonic frequencies. Nevertheless, not necessarily all the frequencies of the N feeding signals should be non-harmonic, as it will be later shown. Let us next gain insight on the dependence of the resonance frequencies of the SIR with its topology.

Figure 2 depicts the two canonical SIR topologies, as well as the topology of the conventional half-wavelength resonator (the relevant electrical parameters are indicated). Note that the two considered topologies are symmetric, corresponding to the SIRs of the encoders proposed in the present paper. The conventional half-wavelength resonator exhibits the fundamental resonance at the frequency f_0 providing an electrical length of 180º (or a half wavelength), and the harmonic frequencies are located at the even and odd multiples of f_0, i.e., $2f_0$, $3f_0$, $4f_0$, … By contrast, in the SIR resonator, the resonance frequencies are no longer multiples of the fundamental one. To demonstrate this, let us calculate the impedance seen from the central (symmetry) plane of the SIR looking at any of the open-ended terminations, Z_{in}, see Fig. 2. Such impedance is given by [51],[52]

$$Z_{in} = j\frac{Z_2 \tan\phi_1 \tan\phi_2 - Z_1}{\tan\phi_1 + K\tan\phi_2} \tag{4}$$

where $K = Z_1/Z_2$ is the impedance contrast of the SIR, Z_1 and Z_2 being the impedances of the line sections, as depicted in Fig. 2, and ϕ_1 and ϕ_2 the corresponding electrical lengths. In (4), losses are excluded, and the influence of the step discontinuity and edge capacitance of the open end is ignored. The SIR resonances are given by those frequencies satisfying either $Z_{in} = 0$ or $Z_{in} = \infty$. In the former case ($Z_{in} = 0$), the resonance condition writes as follows

$$\tan\phi_1 \tan\phi_2 = K \tag{5}$$

For $Z_{in} = \infty$, the following result is obtained

$$\tan\phi_1 = -K\tan\phi_2 \tag{6}$$

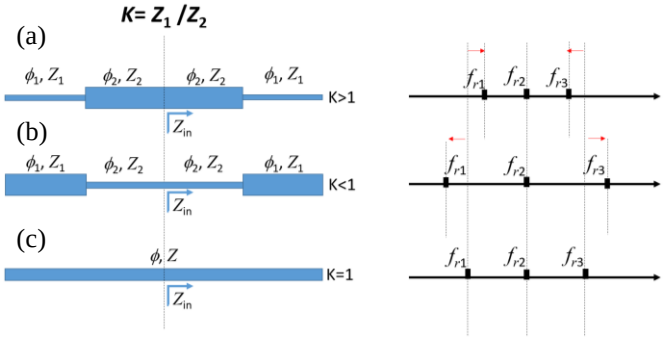

Fig. 2. Canonical topologies of the SIR and half-wavelength resonator, and resonance frequencies. (a) SIR with impedance contrast K >1; (b) SIR with impedance contrast K < 1; conventional half-wavelength resonator (or SIR with impedance contrast K = 1).

Let us next consider two situations, i.e., $K < 1$ and $K > 1$, and let us assume that $\phi_1 = \phi_2 = \phi$ (this latter assumption does not represent a loss of generality, but makes the analysis simpler, and has been adopted in the SIRs of the considered encoders).

In the former case ($K < 1$), the fundamental resonance (with $Z_{in} = 0$) occurs for $0 < \phi < \pi/4$, since $\tan^2 \phi = K < 1$. However, the second resonance frequency (with $Z_{in} = \infty$) takes place for $\phi = \pi/2$, so that the total electrical length of the SIR is 2π at that frequency, i.e., identically to the second resonance of the conventional half-wavelength resonator (or SIR with $K = 1$). For the third resonance frequency (where, again, $Z_{in} = 0$), the phase should satisfy $3\pi/4 < \phi < \pi$ (so that $\tan^2 \phi = K < 1$).

Thus, according to these phases, it follows that for $K < 1$, the fundamental resonance frequency is smaller than half the second resonance frequency, whereas the third resonance frequency is larger than 1.5 times the second resonance frequency. In other words, the first and third resonance frequencies are more distant from the second resonance frequency than in the case of the conventional half wavelength resonator.

For $K > 1$, the fundamental resonance (with $Z_{in} = 0$) occurs for $\pi/4 < \phi < \pi/2$, since $\tan^2 \phi = K > 1$. Similarly, to the previous case ($K < 1$), the second resonance frequency (with $Z_{in} = \infty$) occurs when $\phi = \pi/2$. Finally, for the third resonance frequency, the phase should satisfy $\pi/2 < \phi < 3\pi/4$ (so that $\tan^2 \phi = K > 1$). Thus, for $K > 1$, the proximity of the first and third resonance frequencies to the second one follows an opposite trend to that for $K < 1$.

Figure 2 also depicts (schematically) the separation of the first three resonance frequencies for the SIR with $K < 1$ and with $K > 1$, and for the conventional half-wavelength resonator ($K = 1$). The main conclusion is that, depending on the impedance contrast, K, these frequencies are multiples ($K = 1$), are expanded ($K < 1$), or are constrained ($K > 1$), as it can be graphically appreciated in Fig. 2. This possibility of tailoring the relative position of the resonance frequencies in the SIR makes this resonator useful for the implementation of the electromagnetic encoders of this paper, an aspect to be discussed next.

Let us consider the systematic design of an SIR based encoder with $N = 3$ feeding signals [and $n = 2.81$ bits per encoder row, see (2)]. The three frequencies are tuned to $f_1 = 1$ GHz, $f_2 = 2.5$ GHz, and $f_3 = 4$ GHz. The 7 different frequency combinations, or states, are depicted in Fig. 3, together with the specific types of SIRs considered for their excitations (with $K = 1$, $K < 1$, or $K > 1$). For the state [f_1], an SIR with $K < 1$ is considered, and such SIR is tuned to exhibit the second resonance at 3 GHz. Thus, there exists an impedance contrast $K < 1$ that generates a resonance at $f_1 = 1$ GHz and another one at 5 GHz. Hence, only the resonance f_1 is excited. For the state [f_2], a conventional half-wavelength resonator ($K = 1$) with the first resonance tuned to $f_2 = 2.5$ GHz is used. Note that the second and third resonances of such resonator are 5 GHz and 7.5 GHz, respectively, and therefore, only f_2 is excited. The state [f_3] is generated with a half-wavelength resonator with the fundamental resonance frequency tuned to $f_3 = 4$ GHz (the second and third frequency are 8 GHz and 12 GHz, respectively). The state [f_1, f_2] is generated with an SIR with $K > 1$, with the second resonance tuned to $(f_1 + f_2)/2 = 1.75$ GHz. By conveniently choosing K, the frequencies $f_1 = 1$ GHz ad $f_2 = 2.5$ GHz, equidistant from $(f_1 + f_2)/2 = 1.75$ GHz, are generated. The additional generated frequencies are 1.75 GHz, 3.5 GHz and 4.5 GHz, which do not coincide with f_3. The state [f_1, f_3] is obtained by means of a half-wavelength resonator tuned to $f_1 = 1$ GHz. Note that the frequency $f_3 = 4$ GHz, a multiple of f_1, is also generated (plus the frequencies of 2 GHz and 3 GHz, not of interest). The state [f_2, f_3] is generated with an SIR with $K > 1$ and the second resonance tuned to $f_3 = 4$ GHz. With the adequate value of K, frequencies located at $f_2 = 2.5$ GHz and 5.5 GHz are also generated (the later not being of interest). Finally, the last state ([f_1, f_2, f_3]) is achieved by means of an SIR with $K < 1$ and the second resonance tuned to $f_2 = 2.5$ GHz. It is obvious that with the proper K value, the frequencies $f_1 = 1$ GHz and $f_3 = 4$ GHz, equidistant from f_2, are also generated.

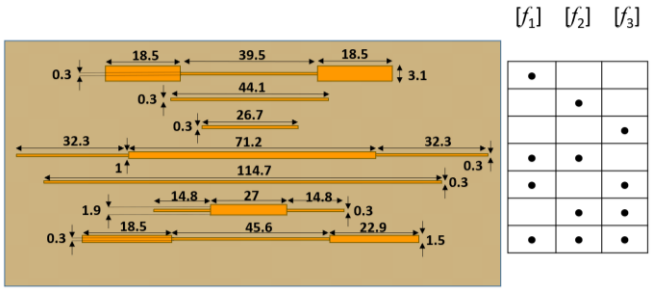

Fig. 3. States for the considered SIR-based electromagnetic encoder, with a reader fed by means of $N = 3$ single-tone signals tuned to $f_1 = 1$ GHz, $f_2 = 2.5$ GHz, and $f_3 = 4$ GHz, and the associated SIRs (or half-wavelength resonators). Dimensions are given in mm.

The dimensions of the layout of the different resonators generating the above-cited states are also included in Fig. 3. The considered substrate for encoder implementation is the *Rogers RO4003C*, with dielectric constant $\varepsilon_r = 3.55$, thickness $h = 0.813$ mm, and loss tangent $\tan\delta = 0.0022$. The reader was implemented in an identical substrate, and the air gap, or vertical distance between the encoder and the reader was set to 0.5 mm. Note that the resonance frequencies of the SIRs and half-wavelength resonators depend not only on the encoder substrate, but also on the air gap distance, and reader substrate.

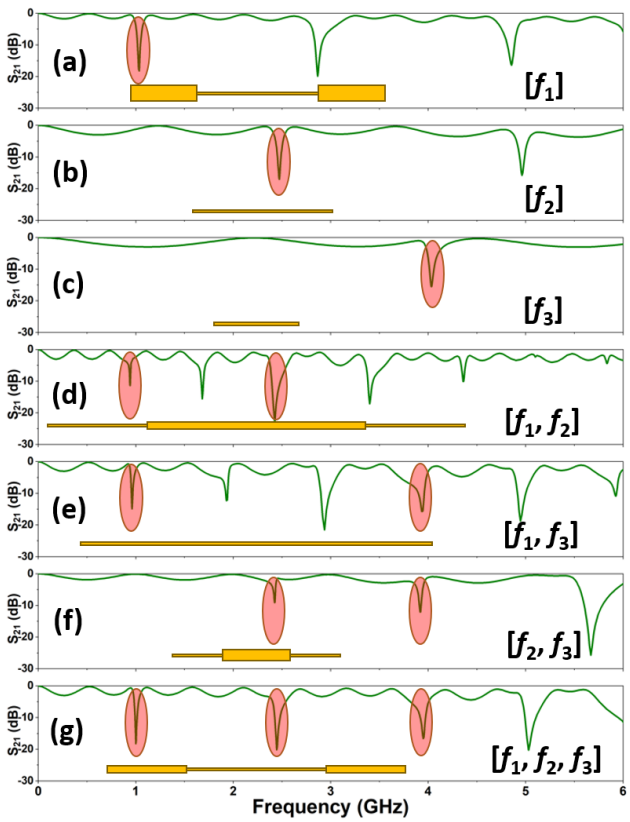

Fig. 4. Simulated responses (magnitude of S_{21}) of the reader line loaded with the different resonators designed to generate the 7 states of the electromagnetic encoder. (a) [f_1]; (b) [f_2]; (c) [f_3]; (d) [f_1, f_2]; (e) [f_1, f_3]; (f) [f_2, f_3]; (g) [f_1, f_2, f_3].

(a)

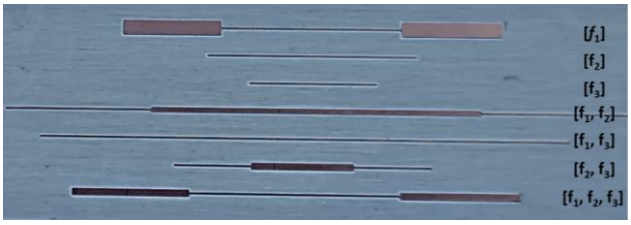

(b)

Fig. 5. Photograph of the fabricated reader (a) and encoder with N = 3 (or n = 2.81 bits per row) and 7 different resonators (b).

The reader is simply a uniform transmission line implemented in the above cited substrate. The width of such line was set to W = 0.5 mm, corresponding to a characteristic impedance of Z_c = 97 Ω, whereas the length was set to L = 190 mm, i.e., the reader line is longer than the longest encoder resonator. It should be mentioned that a narrow reader line is convenient to decrease the period of the encoder (or separation between adjacent resonators), and properly discriminate the states of adjacent resonators.

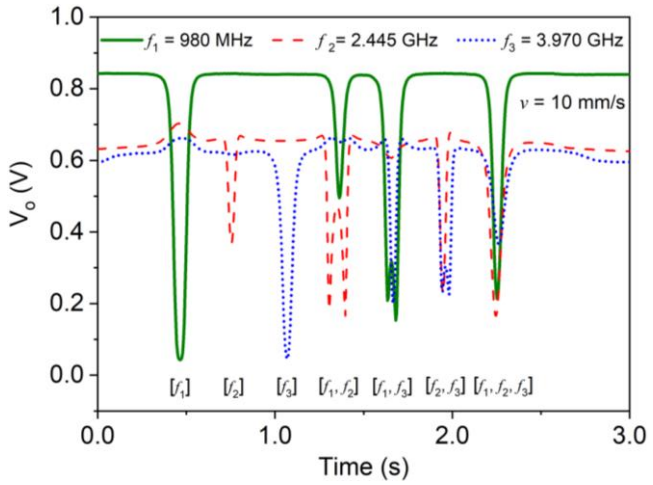

Fig. 6. Envelope functions for the three feeding frequencies of the reader, when the encoder of Fig. 5 is displaced over the reader line. The encoder velocity was set to 10 mm/s. Some tuning in the frequencies of the feeding signals has been necessary due to fabrication related tolerances.

Before the experimental validation, left for the next section, we have simulated the responses of the reader line loaded with the 7 different resonators (with the resonator axis perfectly aligned with the axis of the reader line and with the afore-mentioned air gap). The considered electromagnetic simulator is the *Keysight Momentum* commercial software. The results, depicted in Fig. 4, reveal that the frequencies of the different states are excited. Such frequencies are the notch frequencies of the transmission coefficient, S_{21}, of the reader line, and are indicated in the figure. Certain detuning is unavoidable in practice, but it can be tolerated (an aspect that will be clear in the next section, where experimental validation is carried out).

IV. Experimental Validation

A. Validation by Independently feeding the reader line with the harmonic signals.

Figure 5 depicts the photograph of the fabricated reader and an electromagnetic encoder with 7 rows (and hence 7 resonators), so that all possible encoder resonators are present and do not repeat. Fabrication was carried out by means of the *LPKF H100* drilling machine, available in our laboratory. In this first experiment, devoted to demonstrating the proof-of concept of these encoders, rather than validation by considering the complete system of Fig. 1, we have independently fed the reader line with the three single-tone signals, with frequencies f_1 = 1 GHz, f_2 = 2.5 GHz, and f_3 = 4 GHz. For each frequency, generated by means of the network analyser model *N5221A* as signal generator, we have displaced the encoder over the reader by means of the *Thorlabs LTS300/M* linear displacement system. The amplitude of the output voltage has been retrieved by means of an envelope detector (a Schottky diode model *Avago HSMS- 2860* and a *N2795A* active probe) and visualized in an oscilloscope (model *MSO-X 3104A*).

The envelope functions corresponding to the three frequencies are depicted in Fig. 6, where it can be appreciated that the 7

frequency combinations generated by the corresponding resonators are obtained (identified by the dips in the envelope functions). Such combinations are indicated in Fig. 6 and the corresponding resonators are identified in Fig. 5. Note that the base (voltage) level of the envelope function is different for the three frequencies (roughly 0.84 V, 0.63 V, and 0.60 V for f_1, f_2, and f_3, respectively). The reason is that the reader line is not matched to the impedance of the ports (i.e., $Z_c > Z_0 = 50\Omega$). Under these circumstances, the signal is not totally transmitted to the output port when the resonators do not lie on top of the reader line (i.e., with the resonator and line axis aligned), unless the electrical length of the line is a multiple of 180º (for these phases, the line exhibits total transmission regardless of its characteristic impedance). Indeed, the magnitude of the transmission coefficient with the reader line and the encoder resonators misaligned depends on the electrical length of the line, and hence on the frequency of the feeding signal. This explains the different base levels in the envelope function (directly correlated with the transmission coefficient) for the three frequencies.

Note that the encoder system of Fig. 5 is intrinsically synchronous since the state corresponding to the absence of resonator is not considered (for that reason, the number of bits, n, dictated by expression (2), is slightly inferior to N). This means that any time a resonator crosses the line axis, an ID code

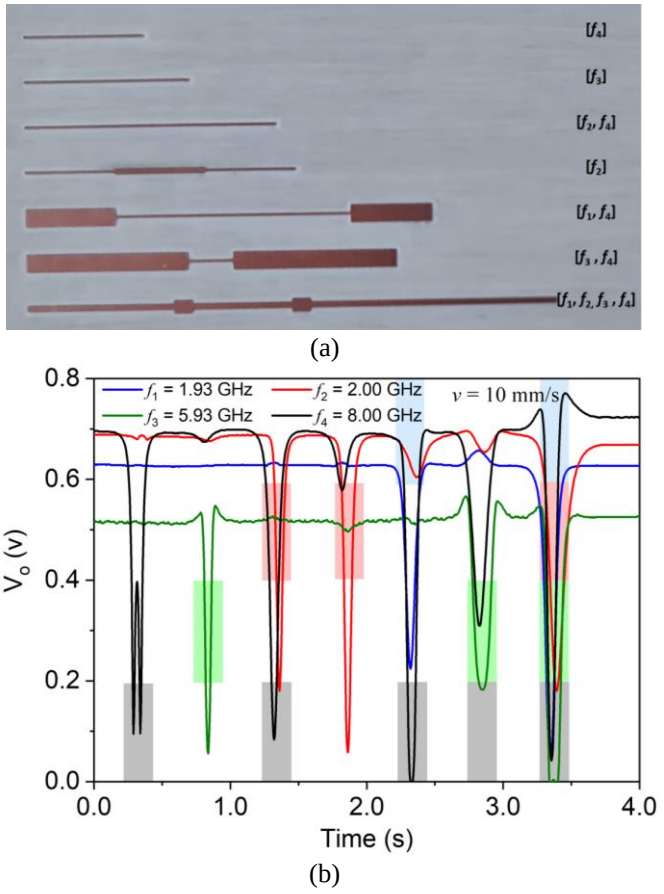

Fig. 7. (a) Photograph of an encoder with 7 different states in the seven encoder rows; (b) envelope functions for the four feeding frequencies of the reader, when the encoder is displaced over the reader line. The encoder velocity was set to 10 mm/s.

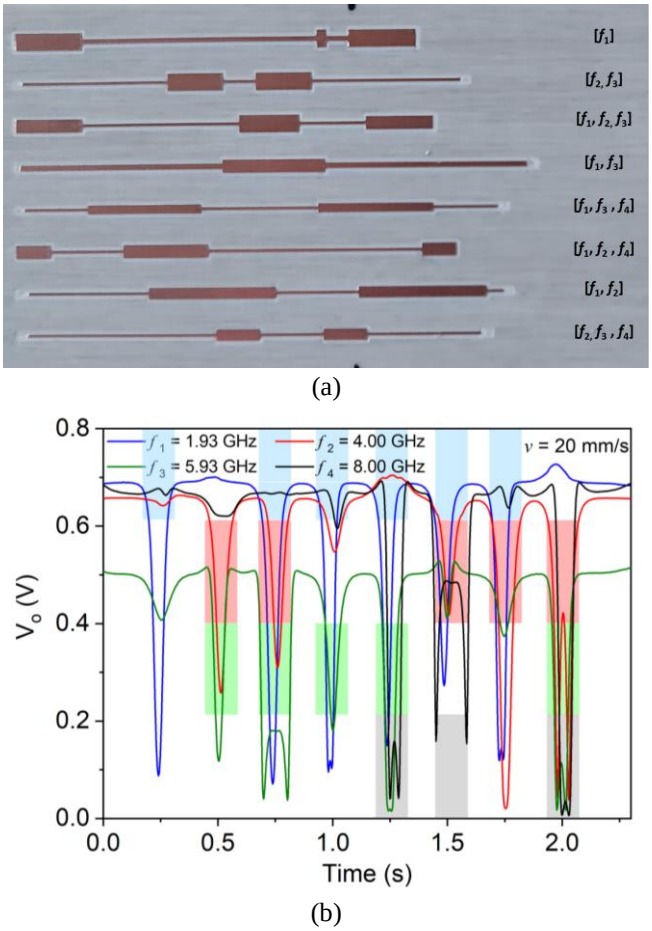

Fig. 8. (a) Photograph of an encoder with 8 different states in the eight encoder rows; (b) envelope functions for the four feeding frequencies of the reader, when the encoder is displaced over the reader line. The encoder velocity was set to 20 mm/s.

corresponding to that encoder row is generated and manifested by the presence of at least one dip in the envelope function (see Fig. 6). It is not necessary to generate a clock signal for synchronization, as it is required in other reported electromagnetic encoders based on binary schemes (e.g., [35]). Obviously, according to (2), as N increases, n approaches N.

Let us next report another prototype electromagnetic encoder, also synchronous, with $N = 4$ feeding frequencies (f_1, f_2, f_3, f_4), and $n = 3.91$ bits per encoder period (or 15 different states). The main difference, as compared to the previous encoder, is that in this encoder, the design of the 15 different resonators (providing the required 15 frequency combinations) has not been done systematically, but according to a tuning and optimization procedure, where each resonator topology has been tailored to achieve the required state. Moreover, certain SIRs of such encoder exhibit more than three sections, and are not necessarily symmetric. The substrate of the reader and encoder are identical to those in reference to the previous encoder. We have fabricated two encoders covering all the states (or frequency combinations). The photographs of these encoders and the corresponding envelope functions are depicted in Figs. 7 and 8, where a good correlation between the dips in the envelope functions and the frequencies generated by the resonators has been found. Note that in these measurements the

encoder velocities are deliberately different (namely 10 mm/s and 20 mm/s) to ensure that system functionality and robustness do not depend on such velocity.

B. Validation by simultaneously feeding the Reader line with the harmonic signals.

Let us next go one step further to validate the proposed system by simultaneously injecting the feeding harmonic signals to the reader line. According to the sketch of Fig. 1, the microcontroller provides different voltage levels to the VCO (those that are needed to generate the required harmonic signals) during different periods of time, so that the harmonic signals are alternately injected to the reader line in a time-division multiplexing scheme. The sketch of Fig. 1 is the best option, since a single VCO is used. However, a VCO covering the required harmonic signals is needed, and this option is not always possible. Due to the lack of an available VCO satisfying this demand in our laboratory, we have opted for an alternative scheme, that uses three independent signal sources and a switch managed by the microcontroller, as depicted in Fig. 9. Note that this validation corresponds to the case with $N = 3$. In particular, one of such sources is a VCO, model *HMC391LP4*, that provides the signal tuned to $f_3 = 3.97$ GHz. The signal tuned to $f_2 = 2.44$ GHz is generated by a vector network analyzer (*Agilent N5221A*), and, finally, the signal tuned to $f_1 = 0.98$ GHz is generated by means of a signal source (*PROMAX GR-405*).

The microcontroller (model *Arduino UNO R3*) generates a cycle of 100 ms, so that during 25 ms each harmonic signal is sequentially injected to the reader line (and during 25 ms no signal is injected to the reader line). Such 100-ms cycle should be small enough as compared with the time lapse between the crossings of two adjacent resonant elements (SIRs) over the axis of the reader line, a necessary requirement. The output signal (i.e., the one recorded at the output port of the envelope detector) is depicted in Fig. 10 (such envelope detector is different to the one used in Section IV.A, in particular, we have used the *Analog Devices* envelope detector, model *ADL5511*). This signal contains the equivalent information to the one that results by independently injecting the harmonic signals (Fig. 6) but multiplexed in time. To better appreciate this time-division multiplexing, we have zoom in Fig. 10 in the vicinity of different instants of time. The results are depicted in Fig. 11. The levels indicated in red correspond to the base levels at different frequencies, after the envelope detector, when there is no resonator on top of the reader line, whereas those in green correspond to the displacement of the encoder over the reader line. It can be appreciated in Fig. 11 that, depending on the resonator that crosses the line, such levels are modified (decrease). For example, in Fig. 11(a), frequencies 0.98 GHz, 2.44 GHz and 3.97 GHz are detected (corresponding to resonators [f_1, f_2, f_3]), whereas in Fig. 11(b), the detected frequency is only [f_3]. In Fig.11(b), we have further zoomed a section containing about 200 ms to help the reader to have a better view of the signals and pulses. Note that the considered envelope detector provides a base signal of roughly 1.20 V when there is no signal at the input port of the reader line. In view of the results of Fig. 10 and 11, it is apparent that such level varies as dictated by the signal tuned to 3.97 GHz. This is attributed to a lack of isolation of the switch, but it does not

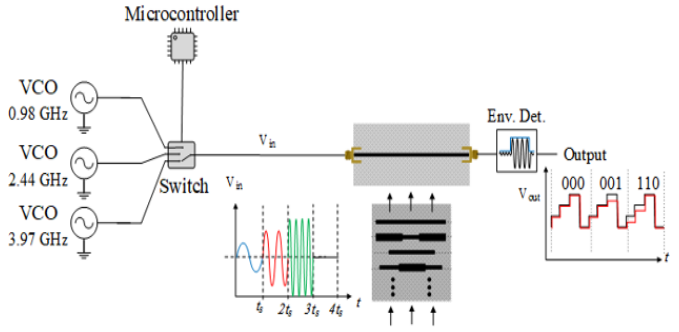

(a)

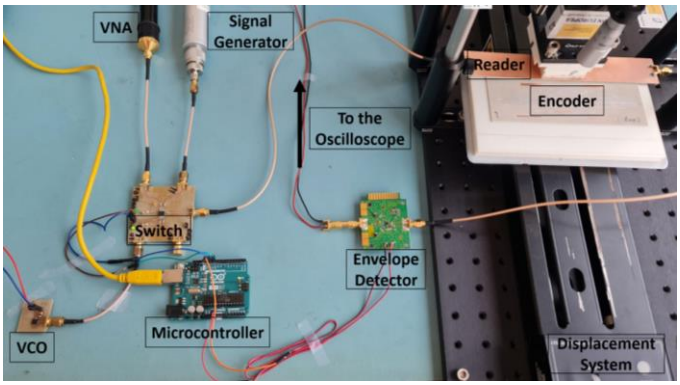

(b)

Fig. 9. Sketch of the system used for validation purposes with simultaneous signal feeding (a) and photograph of the experimental setup (b).

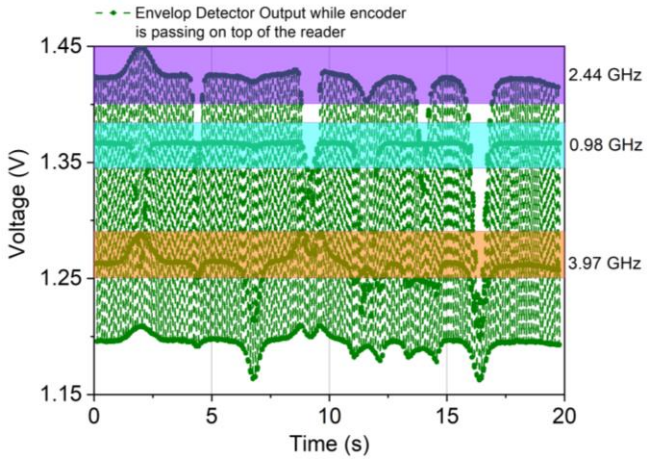

Fig. 10. Signal at the output port of the envelope detector, recorded with an oscilloscope, when the encoder of Fig. 5 crosses the reader line. The encoder velocity was set to 2.5 mm/s.

represent an issue, since this signal is not used, as it does not provide useful information.

The results presented in Figs. 10 and 11 correspond to a sensing experiment where the encoder is displaced over the reader line, and the signal at the output port contains the information regarding the relative position between the reader line and the encoder, determined by the specific ID code, indicated in Fig. 10. Further post-processing to retrieve the specific distance in cm can be added, but this aspect is out of the scope of this paper.

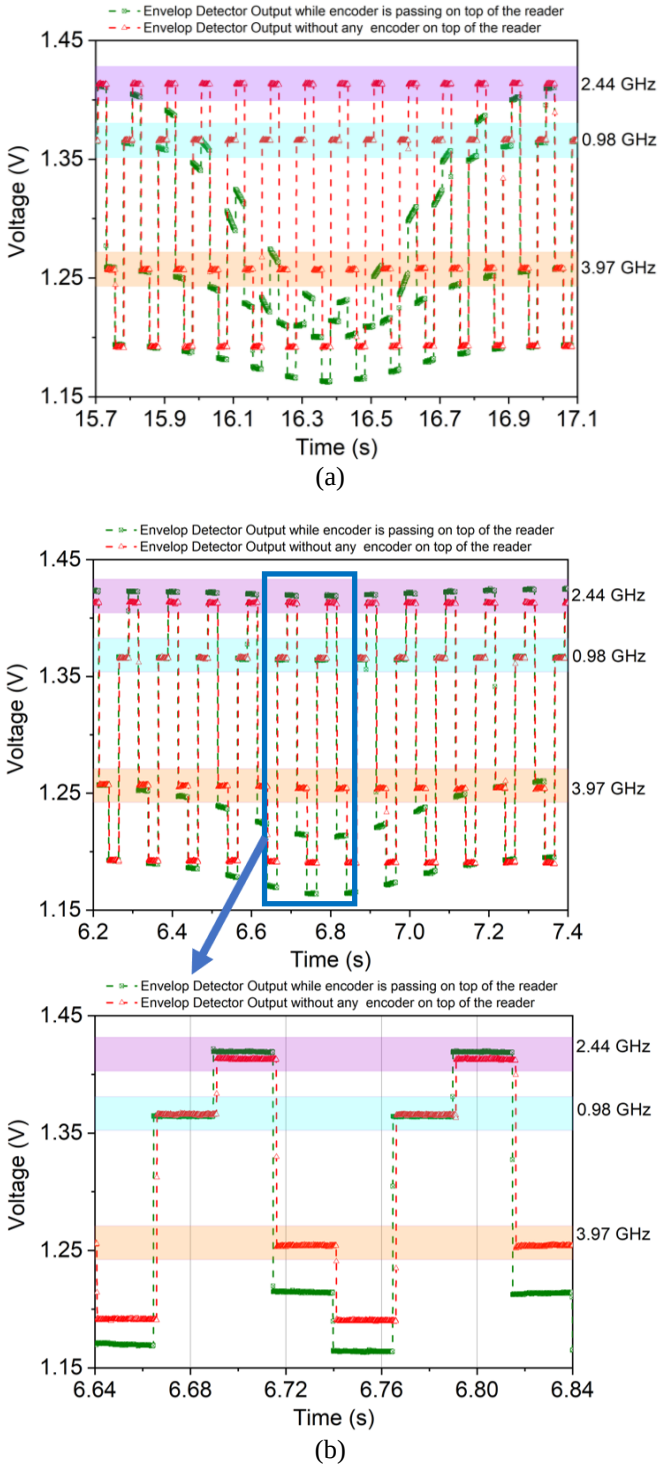

Fig. 11. Zoon view of Fig. 10 in the vicinity of 16 s (a) and 7 s (b).

V. Comparison with other electromagnetic encoders and discussion

Table I compares the electromagnetic encoders of this paper with other previously reported electromagnetic encoders. As already pointed out, the main advantageous aspect of the proposed electromagnetic encoders is the achievable number of bits per encoder period or row (n = 3.91 bits in one of the reported prototypes), and the simplicity of the reader (a transmission line fed by several single-tone signals). In [46]-[48], the number of bits per row is higher than in the prototypes of this work, but at the expense of complex readers, based on power splitter structures or multiple reader lines. The prototype reported in [49] is very competitive, with 4 bits per encoder period, operation at a single frequency, and a simple reader based on a one-port transmission line terminated with a matched load. Such system encodes the information in the phase of the reflection coefficient at the operating frequency (determined by the transverse position of the encoder inclusions). Therefore, retrieving the ID code in operational environment is not absent of certain difficulty. As reported in [49], a gain/phase detector (to provide the phase information) and a specific microwave circuit based on a pair of rat-race hybrid couplers (to separate the feeding signal to the reader from the reflected one) are needed. By contrast, in the system reported in this work, a simple amplitude detector suffices, since the ID information is contained in the envelope function of the transmitted signals.

TABLE I
Comparison of various electromagnetic encoder systems

Ref.	Sync.	Res. (mm)	Bits per row	Single frequency	DPS (bits/cm^2)	DPL (bits/cm)
[53]	Yes	16.0	1	No	0.60	0.63
[54]	Yes	6.0	1	No	1.15	1.67
[55]	Yes	6.0	1	No	1.19	1.67
[35]	Yes	4.0	1	No	0.76	2.50
[56]	Yes	1.2	1	No	1.63	6.96
[37]	Yes	4.0	1	No	0.8	2.50
[38]	Yes	4.0	1	No	0.8	2.50
[43]	Yes	8.0	2	No	0.89	2.50
[33]	No	0.6	1	Yes	7.45	16.7
[34]	No	0.6	1	Yes	26.0	16.7
[57]	No	0.6	1	No	4.90	16.7
[44]	Yes	4.0	2	No	1.67	5.00
[45]	Yes	2.0	2	No	3.34	10.0
[46]	Yes	6.5	4.58	No	0.70	4.58
[47]	Yes	3.0	8.78	No	1.90	29.26
[48]	Yes	5.0	5.58	No	2.32	11.16
[49]	Yes	7.0	4	Yes	0.57	5.71
T.W.*	Yes	5.0	3.91	No	1.11	7.82

*The encoder of this work (T.W.) considered in the table is the one with N = 4 feeding signals.

Encoder resolution (p = 5.0 mm in the reported encoders) is comparable to that of other synchronous electromagnetic encoders with multiple bits per row. With such resolution and number of bits per row, the resulting density of bits per encoder length is found to be DPL = 7.82 bits/cm (prototype with N = 4). The density of bits per surface is DPS = 1.11 bits/cm^2, a relatively low value caused by the width of the encoder. Nevertheless, such width, and hence the DPS, is not critical in many applications. Note that by merely increasing the operational frequencies, the lengths of the SIRs and half-wavelength resonators are dropped down, and this intrinsically improves the DPS. For improving the DPL, either the encoder period is reduced, or the number of bits per row, n, is increased. The period is mainly dictated by the minimum distance between

adjacent resonators necessary to discriminate their respective ID codes (coupling between the line the two encoder resonators, or between adjacent resonators, should be avoided), and such period cannot be reduced substantially, unless all encoder and reader dimensions, including also the air gap, are scaled down (with the penalty of an increase in the feeding frequencies). To increase the number of bits per row, a double-chain encoder (with the resonators of either chain perfectly aligned) and two aligned reader lines constitutes an option, similar to the one reported in [48]. By this means, the number of bits per row and the DPL can be enhanced by a factor of two, with no significant effect on the DPS.

The accuracy, or degree of closeness to the true value of the measurand (the relative distance between the reader and the encoder, in our case.), is an important parameter in sensors. The dips in the time responses determine the instants of time where a resonant element of the encoder is just on top of the reader line, and from the retrieved ID code the absolute position can be determined. There are positions where the reader line is in between resonant elements. Such positions are undetermined and for this reason the resolution of the device is given by the distance between adjacent resonators, or period, p = 5.0 mm, in our case. Such resolution is thus the maximum error in the reported system (note that the error is the opposite of accuracy). Thus, the accuracy is intimately related to the resolution. Optical encoders (either linear or angular) commercially available exhibit, in general, better resolution than the proposed electromagnetic encoder (typically in the submillimetre range). However, optical encoders suffer from other drawbacks, as mentioned before, particularly, higher cost and limited robustness when they operate in environments subjected to pollution or dirtiness. In this paper, the main goal has been to demonstrate the possibility of implementing electromagnetic encoders, as an alternative to optical encoders, with multiple bits per position, pursuing the implementation of absolute encoders, or at least quasi-absolute encoders (depending on the required dynamic range). In terms of performance, particularly resolution, certainly optical encoders are preferred over electromagnetic encoders, but we do consider that our research is of interest given the advantageous aspects of electromagnetic encoders.

Another important parameter is precision (or repeatability), related to the standard deviation of measured data. This performance parameter is determined in our case by the width of the dips in the responses. Note that an estimate of precision is given by the product of the encoder velocity times the width of the dips, given by the width at half maximum. The encoder velocity is the ratio between the period (or resolution), p, and the time interval between adjacent dips, t_{adj}. Let us call the width at half maximum δt. Thus, the precision or uncertainty is given by:

$$d_u = \frac{p}{t_{adj}} \delta t \qquad (7)$$

Although δt and t_{adj} depend on the encoder velocity, its ratio is quite constant, and has been estimated to be roughly 0.26. Thus, according to (7), the precision of the proposed system is roughly d_u =1.3 mm.

These systems can be used as absolute encoder-based linear displacement sensors, where the position is given by the ID code associated to the specific resonator. Naturally, the dynamic range is limited, provided an absolute position system is pursuit. Nevertheless, it is possible to consider quasi-absolute systems where the position is dictated by the ID of that position plus the IDs of a certain number of previous positions (similar to the system of [35]-[39]). By this means, the dynamic range can be dramatically improved. Another potential application concerns the implementation of near-field chipless-RFID systems, where the chipless tags are the encoders, that must be displaced over the reader line to retrieve the whole ID code. As compared to other chipless-RFID systems, typically based on spectral signature barcodes [58]-[70], the proposed electromagnetic encoders, acting as near-field chipless RFID systems, exhibit a relevant advantage: the number of bits is only limited by tag (or encoder) length. However, tag reading proceeds by proximity and alignment with the reader. This aspect is not necessarily an issue in certain applications, such as anti-counterfeiting or secure paper, among others, where reading by proximity might offer a major level of confidence against eavesdropping or spying.

VI. Conclusions

In conclusion, a novel approach for the implementation of synchronous electromagnetic encoders able to provide multiple bits per encoder row has been proposed and validated. The system is compatible with simple readers, consisting merely of a transmission line fed by (roughly) as many single-tone signals, N, as number of bits per row (N = 3 and N = 4 signals in the two reported prototypes). The number of states per row is $2^N - 1$, and such states correspond to any combination of frequencies amongst those of the N feeding single-tone signals. Such frequency combinations are generated in this paper by means of step-impedance resonators (SIRs), i.e., planar resonant elements where the location of the resonance frequencies can be tailored by means of the impedance contrast. Encoder reading is achieved by retrieving the envelope functions of the feeding signals at the output port of the reader line when the encoder is displaced over it at short vertical distance. Good correlation between the ID codes of the different encoder periods (or rows) and the specific encoder resonators of such rows has been found, for both the N = 3 and the N = 4 fabricated prototype encoder systems, thereby validating the proposed approach. Up to date, with such simple reader, synchronous electromagnetic encoders based on frequency encoding exhibiting only 2 bits per row have been reported. This work represents a contribution towards the implementation of true absolute electromagnetic encoders, in which as many number of states per encoder period as different encoder positions are required.

REFERENCES

[1] E. Eitel, "Basics of Rotary Encoders: Overview and New Technologies," *Machine Design Mag.*, vol. 4, no. 2, May. 2014.

[2] G. K. McMillan and D. M. Considine, "Process/Industrial Instrument and Control Handbook," in *Symp. A Quarterly J. In Modern Foreign Literatures*, 1999.

[3] X. Li, J. Qi, Q. Zhang, and Y. Zhang, "Bias-tunable dual-mode ultraviolet photodetectors for photoelectric tachometer," *Appl. Phys. Lett.*, vol. 104, no. 4, paper 041108, Jan. 2014.

[4] F. Martín, C. Herrojo, J. Mata-Contreras, F. Paredes, *Time-Domain Signature Barcodes for Chipless-RFID and Sensing Applications*, Springer, Feb. 2020.

[5] F. Martín, P. Vélez, J. Muñoz-Enano, L. Su, *Planar Microw. Sensors*, Wiley/IEEE Press, Hoboken, NJ, USA, Sep. 2022.

[6] C. Herrojo, F. Paredes, and F. Martín, "3D-printed high data-density electromagnetic encoders based on permittivity contrast for motion control and chipless-RFID", *IEEE Trans. Microw. Theory Techn*., vol. 68, no. 5, pp. 1839-1850, May 2020.

[7] Z. Zhang, Y. Dong, F. Ni, M. Jin, and H. Liu, "A Method for Measurement of Absolute Angular Position and Application in a Novel Electromagnetic Encoder System," *J. Sensors*, vol. Apr. 2015, doi: 10.1155/2015/503852.

[8] Z. Zhang, F. Ni, Y. Dong, M. Jin, and H. Liu, "A novel absolute angular position sensor based on electromagnetism," *Sensors and Actuators, A: Physical*, vol. 194, May. 2013, doi: 10.1016/j.sna.2013.01.040.

[9] J. Jezný, and M. Curilla, "Position Measurement with Hall Effect Sensors", *Am. J. Mech. Eng*., vol. 1, pp. 231–235, Jan. 2013.

[10] P.N. Granell, G. Wang, G. S. Cañon Bermudez, T. Kosub, F. Golmar, L. Steren, J. Fassbender, and D. Makarov, "Highly compliant planar Hall effect sensor with sub 200 nT sensitivity," *Npj Flex. Electron.*, vol. 3, p. 3, Feb. 2019.

[11] A. Lidozzi, L. Solero, F. Crescimbini, and A. Di Napoli, "SVM PMSM Drive with Low Resolution Hall-Effect Sensors," *IEEE Trans. Power Electr*., vol. 22, pp. 282–290, Jan. 2007.

[12] G. Scelba, G. De Donato, G. Scarcella, F. Giulii Capponi, and F. Bonaccorso, "Fault-Tolerant Rotor Position and Velocity Estimation Using Binary Hall-Effect Sensors for Low-Cost Vector Control Drives," *IEEE Trans. Ind. Appl*., vol. 50, pp. 3403–3413, Feb. 2014.

[13] X. Zhang, M. Mehrtash, M.B. Khamesee, "Dual-Axial Motion Control of a Magnetic Levitation System Using Hall-Effect Sensors," *IEEE/ASME Trans. Mechatron*., vol. 21, pp. 1129–1139, Sep. 2015.

[14] G. Liu, B. Chen, and X. Song, "High-Precision Speed and Position Estimation Based on Hall Vector Frequency Tracking for PMSM with Bipolar Hall-Effect Sensors," *IEEE Sens. J*., vol. 19, pp. 2347–2355, Dec. 2018.

[15] Rotary and Linear Motion Sensors. Available online: https://www.rls.si/eng/hilin (accessed on 17 January 2022).

[16] C. Mandel, B. Kubina, M. Schüßler, and R. Jakoby, "Passive chipless wireless sensor for two-dimensional displacement measurement," *41st Eur. Microw. Conf.*, Manchester, UK, Oct. 2011, pp. 79-82.

[17] J. Naqui, M. Durán-Sindreu, and F. Martín, "Alignment and position sensors based on split ring resonators," *Sensors*, vol. 12, pp. 11790-11797, Aug. 2012.

[18] A. Karami-Horestani, C. Fumeaux, S. F. Al-Sarawi, and D. Abbott, "Displacement sensor based on diamond-shaped tapered split ring resonator," *IEEE Sensors J*., vol. 13, no. 4, pp. 1153-1160, Apr. 2013.

[19] A. K. Horestani, J. Naqui, D. Abbott, C. Fumeaux, and F. Martín, "Two-dimensional displacement and alignment sensor based on reflection coefficients of open microstrip lines loaded with split ring resonators," *Electron Lett*., vol. 50, no. 8, pp. 620-622, Apr. 2014.

[20] A. K. Horestani, D. Abbott, and C. Fumeaux, "Rotation sensor based on horn-shaped split ring resonator," *IEEE Sens. J*., vol. 13, pp. 3014-3015, May. 2013.

[21] J. Naqui and F. Martín, "Transmission lines loaded with bisymmetric resonators and their application to angular displacement and velocity sensors," *IEEE Trans. Microw. Theory Techn*., vol. 61, no. 12, pp. 4700-4713, Dec. 2013.

[22] J. Naqui and F. Martín, "Angular displacement and velocity sensors based on electric-LC (ELC) loaded microstrip lines," *IEEE Sensors J*., vol. 14, pp. 939–940, Apr. 2014.

[23] V. Sipal, A. Z. Narbudowicz, and M. J. Ammann, "Contactless measurement of angular velocity using circularly polarized antennas," *IEEE Sensors J.*, vol. 15, no. 6, pp. 3459–3466, Jun. 2015.

[24] A. K. Jha, N. Delmonte, A. Lamecki, M. Mrozowski and M. Bozzi, "Design of Microwave-Based Angular Displacement Sensor," *IEEE Microw. Wireless Compon. Lett*., vol. 29, no. 4, pp. 306-308, Apr. 2019.

[25] C.-H. Chio, R. Gomez-Garcia, L. Yang, K.-W. Tam, W.-W. Choi, and S.-K. Ho, "An angular-displacement microwave sensor using an unequal length-Bi-path transversal filtering section," *IEEE Sensors J*., vol. 20, no. 2, pp. 715–722, Jan. 2020.

[26] A. K. Jha, A. Lamecki, M. Mrozowski and M. Bozzi, "A Highly Sensitive Planar Microwave Sensor for Detecting Direction and Angle of Rotation," *IEEE Trans. Microw. Theory and Techn*., vol. 68, no. 4, pp. 1598-1609, Apr. 2020.

[27] J. Muñoz-Enano, P. Vélez, L. Su, M. Gil, and F. Martín, "A reflective-mode phase-variation displacement sensor", *IEEE Access*, vol. 8, pp. 189565-189575, Oct. 2020.

[28] A. K. Horestani, Z. Shaterian and F. Martín, "Rotation Sensor Based on the Cross-Polarized Excitation of Split Ring Resonators (SRRs)", *IEEE Sensors J.*, vol 20, pp. 9706-9714, Sep. 2020.

[29] A. K. Jha, A. Lamecki, M. Mrozowski and M. Bozzi, "A Microwave Sensor with Operating Band Selection to Detect Rotation and Proximity in the Rapid Prototyping Industry," *IEEE Trans. Industrial Electron*., vol. 68, no. 1, pp. 683-693, Jan. 2021.

[30] S. Harnsoongnoen and N. Angkawisittpan, "Angular displacement sensor based on coplanar waveguide (CPWs) loaded with s-shaped golden spiral-tapered split ring resonators (SGS-SRRs)," *Procedia Comput. Sci*., vol. 86, pp. 75–78, Mar. 2016.

[31] C. H. Chio, R. Gómez-García, L. Yang, K. W. Tam, W. W. Choi and S. K. Ho, "An Angular Displacement Sensor Based on Microwave Transversal Signal Interference Principle," *IEEE Sensors J*., vol. 20, no. 19, pp. 11237-11246, Oct. 2020.

[32] C. Teng, C. H. Chio, K. W. Tam, and P. Y. Lau, "An Angular Displacement Microwave Sensor with 360° Dynamic Range Using Multi-Mode Resonator," *IEEE Sensors J*., vol. 21, no. 3, pp. 2899–2907, Feb. 2021.

[33] C. Herrojo, F. Muela, J. Mata-Contreras, F. Paredes, F. Martín, "High-density microwave encoders for motion control and near-field chipless-RFID", *IEEE Sensors J*., vol. 19, pp. 3673-3682, May 2019.

[34] C. Herrojo, F. Paredes, and F. Martín, "Double-stub loaded microstrip line reader for very high data density microwave encoders", *IEEE Trans. Microw. Theory Techn.*, vol. 67, no. 9, pp. 3527-3536, Sep. 2019.

[35] F. Paredes, C. Herrojo, F. Martín, "Microwave Encoders with Synchronous Reading and Direction Detection for Motion Control Applications", *2020 IEEE-MTT-S Int. Microw. Symp.* (IMS'20), Los Angeles, CA, USA, 21-26 Jun. 2020.

[36] C. Herrojo, F. Paredes, and F. Martín "Synchronism and Direction Detection in High-Resolution/High-Density Electromagnetic Encoders", *IEEE Sensors J*., vol. 21, no. 3, pp. 2873-2882, Feb. 2021.

[37] F. Paredes, C. Herrojo, F. Martín, "3D-printed quasi-absolute electromagnètic encoders for chipless-RFID and motion control applications", *Electronics*, vol. 10, paper 1154, May. 2021.

[38] F. Paredes, C. Herrojo, A. Moya, M. Berenguel-Alonso, D. Gonzalez, J. Bruguera, C. Delgado-Simao, and F. Martín, "Electromagnetic Encoders Screen-Printed on Rubber Belts for Absolute Measurement of Position and Velocity", *Sensors*, vol. 22, paper 2044, Mar. 2022.

[39] F. Paredes, A. Moya, M. Berenguel-Alonso, D. Gonzalez, J. Bruguera, C. Delgado-Simao, and F. Martín, "Motion Control System for Industrial Scenarios Based on Electromagnetic Encoders", *IEEE Trans. Instrum. Meas*., vol. 72, pp. 1-12, Art no. 2003612, 2023.

[40] J. Mata-Contreras, C. Herrojo, and F. Martín, "Application of split ring resonator (SRR) loaded transmission lines to the design of angular displacement and velocity sensors for space applications", *IEEE Trans. Microw. Theory Techn*., vol. 65, no. 11, pp. 4450-4460, Nov. 2017.

[41] C. Herrojo, J. Mata-Contreras, F. Paredes, F. Martín, "Microwave encoders for chipless RFID and angular velocity sensors based on S-shaped split ring resonators (S-SRRs)", *IEEE Sensors J*., vol. 17, pp. 4805-4813, Aug. 2017.

[42] J. Mata-Contreras, C. Herrojo, and F. Martín, "Detecting the rotation direction in contactless angular velocity sensors implemented with rotors loaded with multiple chains of split ring resonators (SRRs)", *IEEE Sensors J*., vol.18, no. 17, pp. 7055-7065, Sep. 2018.

[43] A. Karami-Horestani, F. Paredes and F. Martín, "A Hybrid Time/Frequency Domain Near-Field Chipless-RFID system", *21st Mediterranean Microw. Symp.*, Pizzo Calabro, Italy, May 9-13, 2022.

[44] A. Karami-Horestani, F. Paredes and F. Martín, "Near-Field Hybrid (Time/Frequency Domain) Chipless-RFID System based on Linear Strips Tag", *10th Microw. & RADAR Week*, 12-14 Sep. 2022 Gdansk, Poland.

[45] A. Karami-Horestani, F. Paredes and F. Martín, "Frequency-coded and programmable synchronous electromagnètic encoders based on linear

strips", *IEEE Sensors Lett*., vol. 6, no. 8, pp. 1-4, Art no. 3501704, Aug. 2022.
[46] A. Karami-Horestani, F. Paredes and F. Martín, "Near-Field Chipless-RFID System Based on Hybrid Time/Frequency Domain Encoding and Power Splitter Reader", *52nd Eur. Microw. Conf*., Milan, Italy, 20-25 Sep. 2022.
[47] A. Karami-Horestani, F. Paredes and F. Martín, "High data density absolute electromagnètic encoders based on hybrid time/frequency domain encoding", *IEEE Sensors J*., vol. 22, no. 24, pp. 23866-23876, Oct. 2022.
[48] F. Paredes, A. Karami-Horestani, F. Martín,"Enhanicng the bit density in linear electromagnetic encoders for chipless-RFID and motion sensing applications", *Eur. Conf. on Antennas and Propag.* (EuCAP 2023), Florence, Italy, Mar. 27-31, 2023.
[49] A. Karami-Horestani, F. Paredes, and F. Martín, "Hybrid time/phase domain synchronous electromagnetic encoders for near-field chipless-RFID and motion control applications", *IEEE Trans. Microw. Theory Techn*., to be published.
[50] N.C. de Bruijn, ""Acknowledgement of Priority to C. Flye Sainte-Marie on the counting of circular arrangements of 2n zeros and ones that show each n-letter word exactly once", *T.H.-Report 75-WSK-06*, Technological University Eindhoven, 1975.
[51] D.M. Pozar, *Microwawe Engineering*, 4th Ed., Wiley, Hoboken, USA, Nov. 2011.
[52] J. Naqui, M. Durán-Sindreu, J. Bonache and F. Martín, "Implementation of shunt connected series resonators through stepped-impedance shunt stubs: analysis and limitations", *IET Microw. Ant. Propag*., vol. 5, pp. 1336-1342, Aug. 2011.
[53]. Paredes, C. Herrojo, and F. Martin, "An approach for Synchronous Reading of Near-Field Chipless-RFID Tags", *10th IEEE Int. Conf. on RFID Technol. and Applications* (IEEE RFID-TA 2019), Pisa, Italy, 25-27 Sep. 2019.
[54] F. Paredes, C. Herrojo, and F. Martín, "High Data Density Near-Field Chipless-RFID Tags with Synchronous Reading", *IEEE J. RFID*, vol. 4, no. 4, pp. 517-524, Dec. 2020.
[55] F. Paredes, C. Herrojo, and F. Martín, "Chipless-RFID Sensors for Motion Control Applications", *URSI GASS 2020*, Rome, Italy, 29-5, Aug. 2020.
[56] C. Herrojo, F. Paredes, and F. Martín "Synchronism and Direction Detection in High-Resolution/High-Density Electromagnetic Encoders", *IEEE Sensors J*., vol. 21, no. 3, pp. 2873-2882, Feb. 2021.
[57] J. Havlíček, C. Herrojo, F. Paredes, J. Mata-Contreras, F. Martín, "Enhancing the per-unit-length data density in near-field chipless-RFID systems with sequential bit reading", *IEEE Ant. Wireless Propag. Lett.*, vol. 18, pp. 89-92, Jan. 2019.
[58] I. Jalaly and I. D. Robertson, "RF barcodes using multiple frequency bands," in *Proc. 2005 IEEE MTT-S Int. Microw. Symp. Dig*., Long Beach, CA, pp. 139–142, Jun. 2005.
[59] S. Preradovic, I. Balbin, N. C. Karmakar, and G. F. Swiegers, "Multiresonator-based chipless RFID system for low-cost item tracking," *IEEE Trans. Microw. Theory Techn*., vol. 57, no. 5, pp. 1411–1419, May 2009.
[60] J. McVay, A. Hoorfar, and N. Engheta, "Space-filling curve RFID tags," *Proc. 2006 IEEE Radio Wireless Symp*., pp. 199–202, Oct. 2006.
[61] A. Vena, E. Perret, and S. Tedjini, "A fully printable chipless RFID tag with detuning correction technique," *IEEE Microw. Compon. Lett*., vol. 22, no. 4, pp. 209–211, Apr. 2012.
[62] A. Vena, E. Perret, and S. Tedjini, "Design of compact and autocompensated single-layer chipless RFID tag," *IEEE Trans. Microw. Theory Techn*., vol. 60, no. 9, pp. 2913–2924, Sep. 2012.
[63] A. Vena, E. Perret, and S. Tedjini, "High-capacity chipless RFID tag insensitive to the polarization," *IEEE Trans. Ant. Propag*., vol. 60, no. 10, pp. 4509–4515, Oct. 2012.
[64] M. M. Khan, F. A. Tahir, M. F. Farooqui, A. Shamim, and H. M. Cheema, "3.56-bits/cm^2 compact inkjet printed and application specific chipless RFID tag," *IEEE Ant. Wireless Propag. Lett*., vol. 15, pp. 1109–1112, Oct. 2015.
[65] R. Rezaiesarlak and M. Manteghi, "Complex-natural-resonancebased design of chipless RFID tag for high-density data," *IEEE Trans. Ant. Propag.*, vol. 62, no. 2, pp. 898–904, Feb. 2014.
[66] M. Svanda, J. Machac, M. Polivka, J. Havlicek., "A comparison of two ways to reducing the mutual coupling of chipless RFID tag scatterers," *Proc. 2016 21st Int. Conf. Microw., Radar, and Wireless Commun.* (MIKON), pp. 1–4, May. 2016.
[67] A. Vena, E. Perret, and S. Tedjini, "Chipless RFID tag using hybrid coding technique," *IEEE Trans. Microw. Theory Techn*., vol. 59, no. 12, pp. 3356–3364, Dec. 2011.
[68] M. A. Islam and N. C. Karmakar, "A novel compact printable dual-polarized chipless RFID system," *IEEE Trans. Microw. Theory Techn*., vol. 60, no. 7, pp. 2142–2151, Jul. 2012.
[69] C. Herrojo, F. Paredes, J. Mata-Contreras, S. Zuffanelli, and F. Martín, "Multi-state multi-resonator spectral signature barcodes implemented by means of S-shaped split ring resonators (S-SRR)," *IEEE Trans. Microw. Theory Techn.*, vol. 65, no. 7, pp. 2341–2352, Jul. 2017.
[70] O. Rance, R. Siragusa, P. Lemaître-Auger, and E. Perret, "Toward RCS magnitude level coding for chipless RFID*," IEEE Trans. Microw. Theory Techn*., vol. 64, no. 7, pp. 2315–2325, Jul. 2016.

Amirhossein Karami Horestani has got his bachelor degree at 2015 in the field of biomedical engineering from the University of Isfahan. Then he studies at the University of Tehran in the field of micro/nano electronics for the master's degree until 2018. Since December 2021 he is working on microwave sensors and near-field RFID systems as a PhD student at Universitat Autònoma de Barcelona.

Ferran Paredes (M'14-SM'22) received the Telecommunications Engineering degree from the Universitat Autònoma de Barcelona in 2006 and the PhD degree in Electronics Engineering from the same university in 2012. He is working as a Research Assistant at the Universitat Autònoma de Barcelona and his research interests include metamaterial concepts, passive microwaves devices, antennas, and RFID.

Ferran Martín (M'04-SM'08-F'12) was born in Barakaldo (Vizcaya), Spain in 1965. He received the B.S. Degree in Physics from the Universitat Autònoma de Barcelona (UAB) in 1988 and the PhD degree in 1992. From 1994 up to 2006 he was Associate Professor in Electronics at the Departament d'Enginyeria Electrònica (Universitat Autònoma de Barcelona), and since 2007 he is Full Professor of Electronics. In recent years, he has been involved in different research activities including modelling and simulation of electron devices for high frequency applications, millimeter wave and THz generation systems, and the application of electromagnetic bandgaps to microwave and millimeter wave circuits. He is now very active in the field of metamaterials and their application to the miniaturization and optimization of microwave circuits and antennas. Other topics of interest include microwave sensors and RFID systems, with special emphasis on the development of high data capacity chipless-RFID tags. He is the head of the Microwave Engineering, Metamaterials and Antennas Group (GEMMA Group) at UAB, and director of CIMITEC, a research Center on Metamaterials supported by TECNIO (Generalitat de Catalunya). He has organized several international events related to metamaterials and related topics, including Workshops at the IEEE International Microwave Symposium (years 2005 and 2007) and European Microwave Conference (2009, 2015 and 2017), and the Fifth International Congress on Advanced Electromagnetic Materials in Microwaves and Optics (Metamaterials 2011), where he acted as Chair of the Local Organizing Committee. He has acted as Guest Editor for six Special Issues on metamaterials and sensors in five International Journals. He has authored and co-authored over 650 technical conference, letter, journal papers and book chapters, he is co-author of the book on Metamaterials entitled *Metamaterials with Negative Parameters: Theory, Design and Microwave Applications* (John Wiley & Sons Inc.), author of the book *Artificial Transmission Lines for RF and Microwave Applications* (John Wiley & Sons Inc.), co-editor of the book *Balanced Microwave Filters* (Wiley/IEEE Press), co-author of the book *Time-Domain Signature Barcodes for Chipless-RFID and Sensing Applications* (Springer), and co-author of the book *Planar Microwave Sensors* (Wiley/IEEE Press). Ferran Martín has generated 22 PhDs, has filed several patents on metamaterials and has headed several Development Contracts.
Prof. Martín is a member of the IEEE Microwave Theory and Techniques Society (IEEE MTT-S). He is reviewer of the IEEE Transactions on

Microwave Theory and Techniques and IEEE Microwave and Wireless Components Letters, among many other journals, and he serves as member of the Editorial Board of IET Microwaves, Antennas and Propagation, International Journal of RF and Microwave Computer-Aided Engineering, and Sensors. He is also a member of the Technical Committees of the European Microwave Conference (EuMC) and International Congress on Advanced Electromagnetic Materials in Microwaves and Optics (Metamaterials). Among his distinctions, Ferran Martín has received the 2006 Duran Farell Prize for Technological Research, he holds the *Parc de Recerca UAB – Santander* Technology Transfer Chair, and he has been the recipient of three ICREA ACADEMIA Awards (calls 2008, 2013 and 2018). He is Fellow of the IEEE and Fellow of the IET.